αMI-domain of Integrin Mac-1 Binds the Cytokine Pleiotrophin Using Multiple Mechanisms

Hoa Nguyen[1], Nataly P. Podolnikova[2], Tatiana P. Ugarova[2], and Xu Wang[1]

[1]School of Molecular Sciences and [2]School of Life Sciences, Arizona State University, Tempe, Arizona

Corresponding author: xuwang@asu.edu

Keywords: integrin, macrophages, Mac-1, pleiotrophin, NMR

SUMMARY

The integrin Mac-1 ($\alpha_M\beta_2$, CD11b/CD18, CR3) is an important adhesion receptor expressed on macrophages and neutrophils. Mac-1 is also the most promiscuous member of the integrin family that binds a diverse set of ligands through its α_MI-domain. However, the binding mechanism of most ligands is not clear. We have determined the interaction of α_MI-domain with the cytokine pleiotrophin (PTN), a cationic protein known to bind α_MI-domain and induce Mac-1-mediated cell adhesion and migration. Our data show that PTN's N-terminal domain binds a unique site near the N- and C-termini of the α_MI-domain using a metal-independent mechanism. However, stronger interaction is achieved when an acidic amino acid in a zwitterionic motif in PTN's C-terminal domain chelates the divalent cation in the metal ion-dependent adhesion site of the active α_MI-domain. These results indicate that α_MI-domain can bind ligands using multiple mechanisms, and suggest that active α_MI-domain prefers acidic amino acids in zwitterionic motifs.

HIGHLIGHTS

- α_MI-domain's interaction with the cytokine pleiotrophin (PTN) was investigated with solution NMR.

- α_MI-domain binds PTN using multiple mechanisms.

- PTN's N-terminal domain binds both active and inactive α_MI-domains using a unique site near α_MI-domain's termini.

- PTN's C-terminal domain binds only active α_MI-domain through a metal-dependent interaction.

2

INTRODUCTION

Mac-1 ($\alpha_M\beta_2$, CD11b/CD18, CR3) is a member of the $\alpha\beta$ heterodimeric adhesion receptor family known as integrins. Mac-1 is primarily expressed in neutrophils, monocytes, and macrophages. It is responsible for many important activities in these cells, including phagocytosis, migration, and degranulation (Coxon et al., 1996; Lu and Springer, 1997; Ding et al., 1999; Prince et al., 2001). It has also been increasingly recognized as a vital regulator of the inflammatory state of these cells, capable of promoting both pro-inflammatory and anti-inflammatory pathways in a context dependent way (Rosetti and Mayadas, 2016). Mac-1's diverse biological activities are closely connected with its broad ligand specificity. It is the most promiscuous member of the integrin family and is known to bind nearly 100 different ligands with little consensus among their structures (Lamers et al., 2021). The best-known and most characterized Mac-1 ligands include fibrinogen (Altieri et al., 1990; Ugarova et al., 1998), complement factor C3b (Michishita et al., 1993), and intercellular adhesion molecule 1 (ICAM-1) (Smith et al., 1989; Diamond et al., 1990), and GPIbα (Simon et al., 2000). Still, it is also known to bind such diverse ligands as JAM-3 (Santoso et al., 2002), elastase (Cai and Wright, 1996), myeloperoxidase (Johansson et al., 1997), plasminogen (Lishko et al., 2004), ovalbumin (Zhang and Plow, 1996), keyhole limpet hemocyanin (Shappell et al., 1990; Davis, 1992), CCN1(Schober et al., 2003), and CD40L(Wolf et al., 2011). Recently, it was also shown to bind SIRPα and mediate the merging of macrophages (Podolnikova et al., 2019). Although many ligands are known to bind Mac-1, the binding mechanisms of only a handful of ligands were confirmed with structures (Bajic et al., 2013; Jensen et al., 2016; Morgan et al., 2019; Trstenjak et al., 2020; Fernandez et al., 2022; Goldsmith et al., 2022). The binding interactions of other ligands and their functional consequences remain to be elucidated.

Surprisingly, despite the structural diversity among Mac-1 ligands, most bind to the I-domain of the α_M subunit (α_MI-domain). α_MI-domain is a two hundred residue Rossmann fold domain inserted between blades two and three of α_M's β-propeller. It contains a divalent metal binding site called the metal ion-dependent adhesion site (MIDAS). MIDAS facilitates metal ion-mediated binding of some ligands by allowing the divalent cation in the MIDAS to be chelated by an acidic amino acid in the ligand. The

3

conformation of the α_MI-domain is crucial to the strength of metal-mediated ligand binding. In particular, when the α_MI-domain is in the inactive or "closed" conformation, the coordination of the metal in MIDAS does not allow efficient chelation of the metal ion by the ligand. However, when the α_MI-domain is in the active or "open" conformation, the movement of its C-terminal helix away from MIDAS allows the ligand's acidic amino acid to chelate the metal ion with much higher affinity (Lee et al., 1995).

Although metal-mediated ligand binding is prevalent among integrins, it has long been known that Mac-1 uses other ligand binding mechanisms because some Mac-1-binding sequence motifs do not contain acidic amino acids (Yakubenko et al., 2001). In addition, a systematic peptide screening revealed that motifs containing basic amino acids flanked by hydrophobic amino acids also have a high affinity for α_MI-domain (Podolnikova et al., 2015b). This has led to the discovery of several new integrin ligands, including the cathelicidin peptide LL-37 (Lishko et al., 2016; Zhang et al., 2016), the opioid peptide dynorphin A (Podolnikova et al., 2015a), the chemokine PF4 (Lishko et al., 2018), the cytokine pleiotrophin (PTN) (Shen et al., 2017), and many cationic ligands (Podolnikova et al., 2015b).

PTN is a cytokine consisting of two thrombospondin type-1 repeat domains and plays important roles in cell differentiation and proliferation (Ryan et al., 2016; Wang, 2020). It is also a modulator of microglia activity (Fernandez-Calle et al., 2017; Miao et al., 2019; Linnerbauer et al., 2021), where Mac-1 is highly expressed. Our previous work showed that PTN induced adhesion and migration of various Mac-1-expressing cells, and PTN can activate ERK1/2 in a Mac-1-dependent manner (Shen et al., 2017). As a representative cationic ligand, we wondered if PTN's interaction with α_MI-domain can provide insight into the binding mechanism of this class of ligands. Solution NMR characterization of the interaction of PTN with inactive α_MI-domain showed that the interaction is independent of Mg^{2+} and the binding interface includes the $\alpha5$-$\beta5$ loop of inactive α_MI-domain and PTN's N-terminal domain (PTN-NTD) (Feng et al., 2021). However, these data do not explain the observation that Mg^{2+} ions significantly enhanced the binding of PTN to active α_MI-domain (Shen et al., 2017), implying that a divalent cation-dependent mechanism is also part of the interaction.

In the current study, we investigated PTN's interaction with both active and inactive α_MI-domain. Our data indicate the Mg^{2+}-independent interactions between α_MI-domain and PTN involve a binding interface formed by PTN-NTD and residues from the α5-β5/α6-β6 loops near the termini of α_MI-domain. However, the Mg^{2+}-dependent mechanism uses acidic amino acids in PTN to chelate the metal ion in α_MI-domain's MIDAS. In particular, residue E98 in the PTN's C-terminal domain (PTN-CTD) was shown to be the preferred chelator of MIDAS metal. We attribute this preference to the fact that E98 is part of a zwitterionic motif and its interaction with the metal is stabilized by favorable electrostatic interactions between charged residues around E98 and the MIDAS. Using these data, we created models of the inactive α_MI-domain-PTN-NTD and active α_MI-domain-PTN-CTD complexes using HADDOCK (Dominguez et al., 2003). We also carried out molecular dynamics (MD) simulations of these models to provide additional insights into the mechanism by which the α_MI-domain can interact with its ligands.

RESULTS

Mg^{2+}-independent interactions between PTN and α$_M$I-domain. We have shown previously that although PTN has the highest affinity for active α$_M$I-domain, it also interacts weakly with inactive α$_M$I-domain (Shen et al., 2017). Additional studies showed the metal-independent interaction is mediated by the α5-β5 loop near the termini of inactive α$_M$I-domain and PTN-NTD (Feng et al., 2021). To determine the structure of the inactive α$_M$I-domain-PTN-NTD complex, we collected the F1-^{13}C-edited/F3-^{13}C,^{15}N-filtered HSQCNOESY spectrum of a sample containing 0.2 mM ^{13}C, ^{15}N-labeled inactive α$_M$I-domain and 1.0 mM unlabeled PTN-NTD with no Mg^{2+}. These data revealed many intermolecular contacts between PTN-NTD and inactive α$_M$I-domain (Figure 1). In particular, methyl groups of residue L32 in PTN-NTD had definitive contacts with G263 and I265 in the α5-β5 loop of inactive α$_M$I-domain. In addition, the methyl group of
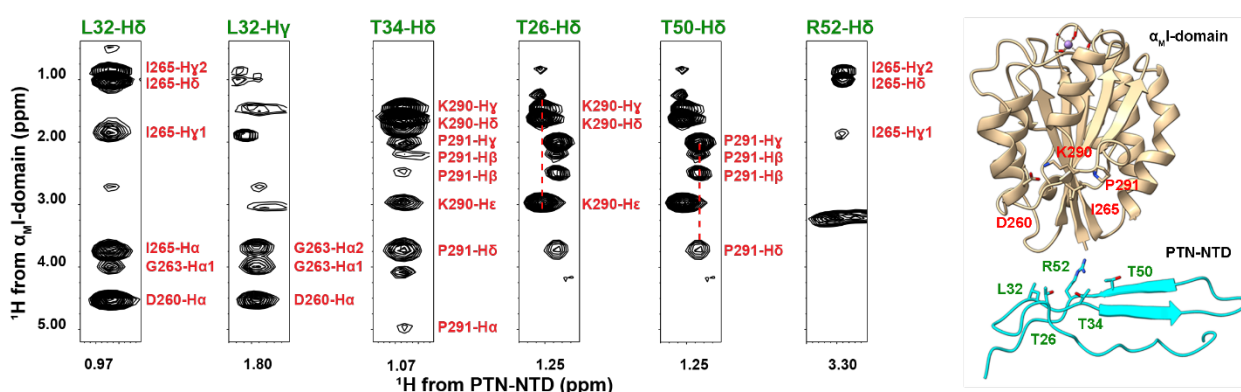

Figure 1. Contacts between the inactive α$_M$I-domain and PTN-NTD. Strips from F1-^{13}C-edited/F3-^{13}C,^{15}N-filtered HSQCNOESY spectrum of ^{13}C,^{15}N-labeled inactive α$_M$I-domain and unlabeled PTN-NTD. Inactive α$_M$I-domain assignments are shown in red. PTN-NTD assignments are shown in green. Ribbon diagram of inactive α$_M$I-domain and PTN-NTD with residues involved in the intermolecular contacts labeled are shown on the right.

residue T26 in PTN-NTD contacted residue K290 in inactive α$_M$I-domain, T34 in PTN-NTD contacted both residues K290 and P291 in inactive α$_M$I-domain, and T50 in PTN-NTD contacted residue P291 in inactive α$_M$I-domain. R52 in PTN-NTD also contacted I265 in inactive α$_M$I-domain. To confirm the assignments of the PTN residues, we collected the F1-^{13}C,^{15}N-filtered/F3-^{13}C-edited NOESYHSQC spectrum of a sample containing 0.2 mM unlabeled inactive α$_M$I-domain and 0.5 mM ^{13}C, ^{15}N-labeled PTN-NTD. These data provided the ^{13}C chemical shifts of the PTN-NTD atoms at the interaction interface (Figure S1). It should be noted that the NMR signal from K290 was mis-assigned to K168 previously (Feng et al., 2021). In the

current study, the assignment of residue K290 in α_MI-domain was confirmed through selective ^{15}N-labeling of lysines and a K290R mutant of inactive α_MI-domain (Figure S2). The ^{15}N-edited NOESYHSQC spectrum of inactive α_M I-domain containing selectively ^{15}N-labeled lysines allowed the side chain hydrogens of lysines to be assigned. K290 was the only lysine whose side chain proton resonance frequencies matched the intermolecular NOE cross peaks in the F1-^{13}C-edited/ F3-^{13}C,^{15}N- filtered HSQCNOESY spectrum. We also acquired an F1-^{13}C-edited/F3-^{13}C,^{15}N-filtered HSQCNOESY spectrum of ^{13}C,^{15}N-labeled inactive α_MI-domain in the presence of PTN-CTD. The data produced no identifiable intermolecular cross peaks between PTN-CTD and inactive α_MI-domain (Figure S3). This is consistent with the observation that only PTN-NTD can produce the large chemical shift perturbations in ^{15}N-HSQC spectrum of inactive α_MI-domain while PTN-CTD induces only minor perturbations. (Feng et al., 2021).

Altogether, these data indicate that the interaction interface between PTN-NTD and inactive α_MI-domain includes the $\alpha5$-$\beta5$ and $\alpha6$-$\beta6$ loops of inactive α_MI-domain and PTN-NTD. In addition, both inactive and the Q163C/Q309C active α_MI-domain (Shimaoka et al., 2002) induced similar chemical shift changes in PTN-NTD (Figure S4). This implies that PTN-NTD most likely has similar metal-independent interactions with active α_MI-domain, suggesting that the Mg^{2+}-independent interaction between PTN and α_MI-domain is not sensitive to the activation state of α_MI-domain.

Mg^{2+}-dependent interactions between α_MI-domain and PTN. Our previous study has shown that PTN's affinity for active α_MI-domain is higher than for inactive α_MI-domain and Mg^{2+} is required for the interaction (Shen et al., 2017). To elucidate the underlying mechanism, we investigated PTN's interaction with the Q163C/Q309C mutant of α_MI-domain, which is forced into the active conformation by a well-placed disulfide bond (Shimaoka et al., 2002). A previous study has shown that the Q163C/Q309C mutant is more suitable for NMR studies because, while it has the same conformation and ligand affinity as active α_MI-domains created by the removal of residue I316 (Xiong et al., 2000), it possesses higher stability and better NMR spectral quality (Nguyen et al., 2023). Because of these favorable properties, the

Q163C/Q309C mutant was chosen for this study. All subsequent mentions of active α_MI-domain in this article refer to the Q163C/Q309C mutant.

Interestingly, when we titrated the active α_MI-domain with PTN in the presence of Mg^{2+}, PTN induced similar spectral changes in active α_MI-domain as glutamate, a ligand known to chelate the metal in the MIDAS of the I316G active α_MI-domain (Vorup-Jensen et al., 2005) (Figure 2A). In particular, adding either glutamate or PTN to the Mg^{2+}-bound active α_MI-domain led to intensity decreases in some signals and the appearance of new signals, consistent with slow time scale exchange between ligand-free and
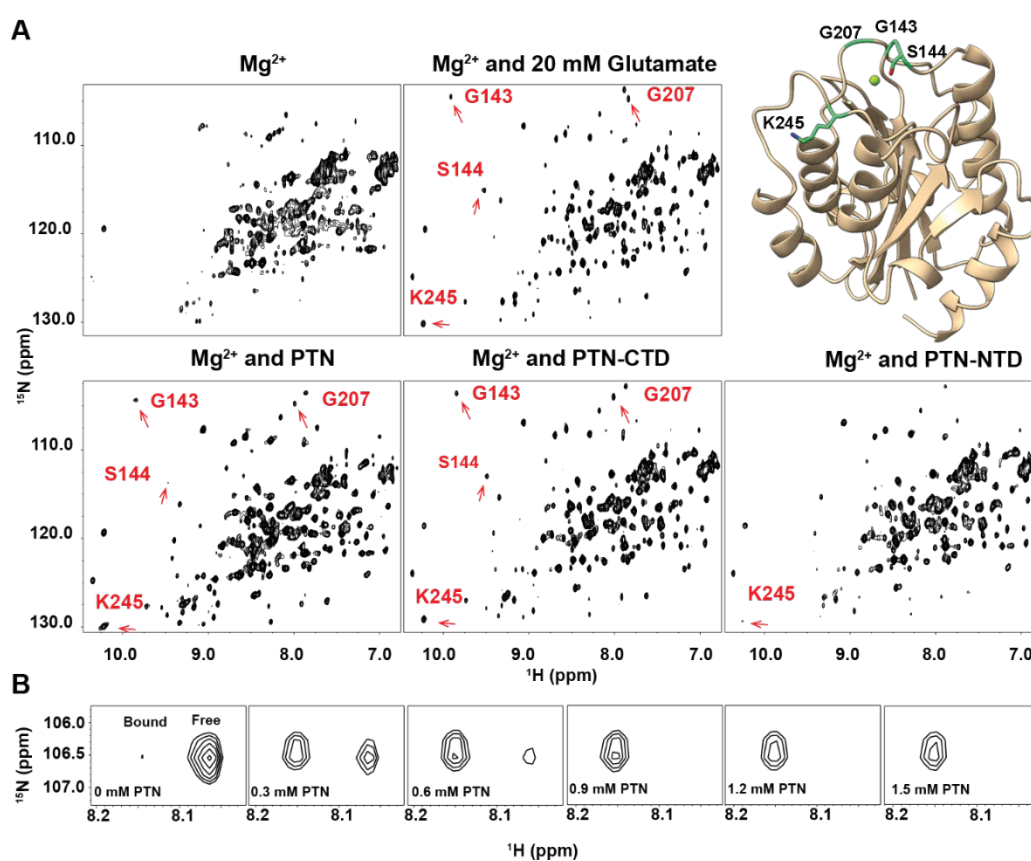

Figure 2. Ligand-induced changes in the ^{15}N-HSQC spectrum of active α_MI-domain. (A) ^{15}N-HSQC of the active α_MI-domain in the presence of different ligands. The changes in the spectrum of active α_M-I domain produced by wild-type PTN or PTN domains are similar to those produced by glutamate, including the appearance of the residues around MIDAS (G143, S144, G207, K245). The signal intensities of the MIDAS residues induced by PTN-NTD were much weaker than those induced by PTN-CTD at the same concentration. Ribbon representation of active α_MI-domain with labeled MIDAS residues are shown on the top right. B) ^{15}N-HSQC signal of residue G228 in Mg^{2+} -saturated active α_MI-domain with different concentrations of PTN. The signal underwent slow time scale exchanges when titrated with PTN.

8

ligand-bound forms of α_MI-domain. Figure 2B shows the signal of residue G228 of α_MI-domain undergoing slow exchange when titrated with PTN. Three of the new signals that appeared in the presence of ligands were assigned to residues G143, S144, and I145, all are residues in one of the MIDAS segments that directly chelate the metal. The similarity in ligand-induced spectral perturbations shows that glutamate and PTN interacted with the MIDAS similarly. This finding supports the idea that PTN binds active α_MI-domain through metal-mediated interactions. Some MIDAS residues also exhibit PTN-domain-specific chemical shifts. In particular, wild-type PTN binding produced two signals from residue S144. However, only one of the signals was seen when PTN-CTD was the ligand whereas PTN-NTD only produced the other signal (Figure S5). We interpret this as an indication that chelation of the metal by different domains resulted in differences in the chemical shifts of the S144 signal. The fact that both signals are present when wild-type PTN is the ligand indicates both PTN-NTD and PTN-CTD can chelate the metal. However, PTN-CTD produced higher intensity signals that are consistent with stable chelation of the MIDAS metal. In contrast, the intensities of these signals were much weaker when PTN-NTD was mixed with active α_MI-domain (Figure 2A). This indicates PTN-CTD may have higher affinity for active α_MI-domain than PTN-NTD. It should also be noted that PTN did not induce these changes in the absence of Mg^{2+} (Figure S6), supporting the idea that the observed active α_MI-domain spectral changes induced by PTN are metal-dependent.

Using intensity increases in the ligand-bound species as a measure of the binding allowed us to obtain the K_d of interaction f by fitting the intensity changes to a one-to-one binding model. We also carried out principle component analysis on the spectral data using the software TRENDNMR (Xu and Van Doren, 2016) and used the magnitude of principle component 1 as a measure of the binding to estimate the K_d of interaction. Figure 3A and Table S1 show K_d s obtained by these analyses. The K_d for glutamate was ~ 5.5 mM, whereas the K_d of interaction for PTN was ~ 0.1 mM, significantly lower than that of the metal-independent interaction (~ 1 mM) (Feng et al., 2021). To determine which domain of PTN is responsible for the metal-dependent interaction, we titrated active α_MI-domain with PTN-CTD and PTN-NTD. The K_d for PTN-CTD binding was ~ 0.1 mM. The K_d for PTN-NTD binding could not be estimated accurately

because of the low intensities of the new ligand-induced signals, but it is at least 9 times greater than the K_d for PTN and PTN-CTD. These results support the conclusion that PTN-CTD contributed more to binding active α_MI-domain through metal-chelation.
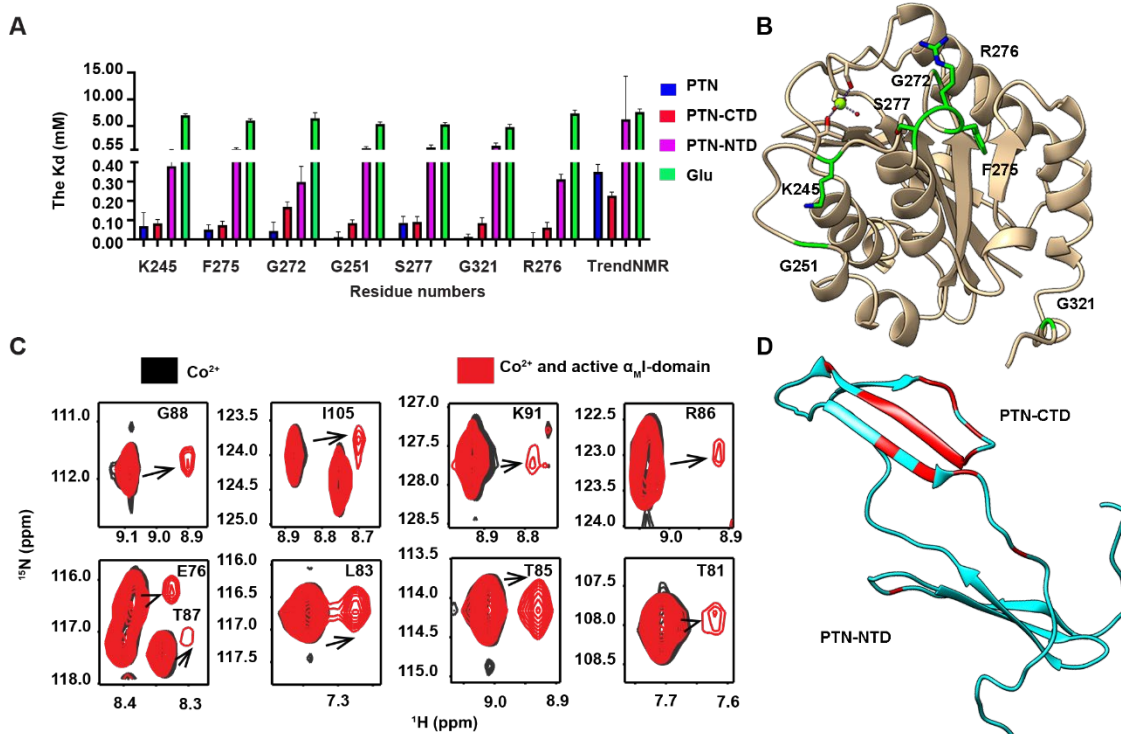

Figure 3: PTN-CTD is the binding site for active α_MI-domain. A) Active α_MI-domain's K_d of binding for wild-type PTN (blue), PTN-CTD (red), PTN-NTD (magenta), and glutamate (green). K_ds were calculated by either fitting the ligand induced signal intensity increases in six residues with high signal-to-noise or using global spectral changes estimated with TrendNMR. Error bars reflect S.D. in data fitting. B) The ribbon representation of active α_MI-domain with residues used to calculate the K_d shown in the stick form. C) ^{15}N-HSQC of PTN in the presence of Co^{2+} (black) and Co^{2+}/active α_MI-domain (red). D) The ribbon representation of PTN with residues exhibiting PCS shown in red. All except two residues exhibiting a PCS peak were located in PTN-CTD.

Another observation supporting PTN-CTD as the dominant metal binding domain is that Co^{2+}-bound active α_MI-domain induced pseudocontact shifts (PCS) mostly in residues from PTN-CTD. The MIDAS of α_MI-domain can chelate paramagnetic Co^{2+} and Co^{2+} bound α_MI-domain retains its ligand affinity (Michishita et al., 1993). The dipole-dipole interaction between the paramagnetic Co^{2+} ion and nearby atoms can induce a change in the chemical shifts of these atoms, commonly referred to as PCS (Nitsche and Otting, 2017). In protein-ligand interactions, the binding of the ligand to a paramagneti metal-containing protein can induce PCS in the ligand, if the interaction is sufficiently rigid. To investigate whether these transferred

10

PCS can be observed in PTN, we collected the spectrum of ^{15}N-labeled PTN in the presence and absence of Co^{2+}-bound active α_MI-domain. The results showed that the presence of Co^{2+}-bound active α_MI-domain induced an additional signal from some PTN residues (Figure 3C). The chemical shift differences between the new and original signals were consistent with diagonal shifts expected of small PCS. Most residues exhibiting a PCS peak were in PTN-CTD (Figure 3D). To confirm these signals resulted from PTN-CTD's binding to Co^{2+}-bound active α_MI-domain, we also collected similar data of PTN-CTD with Mg^{2+}-bound active α_MI-domain and Co^{2+}-bound inactive α_MI-domain. The absence of either Co^{2+} or active α_MI-domain produced no PCS in PTN-CTD (Figure S7). These results support the conclusion that PTN-CTD maintains more stable interactions with active α_MI-domain. It should be noted that the intensities of these PCS signals are only about 11 % of the non-PCS signals, and higher concentrations of α_MI-domain or Co^{2+} did not increase the relative intensities of the PCS signals (data not shown). This implies that PTN-CTD may bind to active α_MI-domain in multiple ways and only some binding modes can induce PCS.

To identify which residue in PTN-CTD chelates the divalent cation in MIDAS, we collected the F1- ^{13}C-edited/F3-^{13}C,^{15}N-filtered HSQCNOESY spectrum of ^{13}C-labeled active α_MI-domain and unlabeled PTN-CTD. However, no intermolecular NOE was observed (Figure S8). This indicates no significant contact exists between the side chains of these proteins. We then collected ^{1}H-^{1}H and ^{1}H-^{13}C projections of the ^{13}C-HSQC-NOESY-^{15}N-HMQC spectrum of a sample containing 1 mM ^{13}C-labeled PTN and 0.25 mM ^{2}H, ^{15}N-labeled active α_MI-domain. Our data showed that several MIDAS residues from active α_MI-domain, including G143, S144, I145, and R208, have intermolecular contacts with a glutamate side chain and the side chain methyl group of A93 in PTN-CTD (Figure 4). Due to chemical shift degeneracy in glutamate side chain atoms, we could not identify the exact glutamate. However, the closest glutamate to A93 is E98. Therefore, we hypothesized that E98 was likely the chelator of the metal ion in MIDAS. We also collected 4D ^{13}C-HSQC-NOESY-^{15}N-HMQC spectrum of ^{2}H, ^{15}N-labeled PTN-CTD in the presence of ^{13}C-labeled active α_MI-domain. However, no intermolecular contacts were detected. These results indicate that while backbone amide hydrogens of active α_MI-domain were at the binding interface, none of the backbone amide hydrogens in PTN-CTD were at the interface.
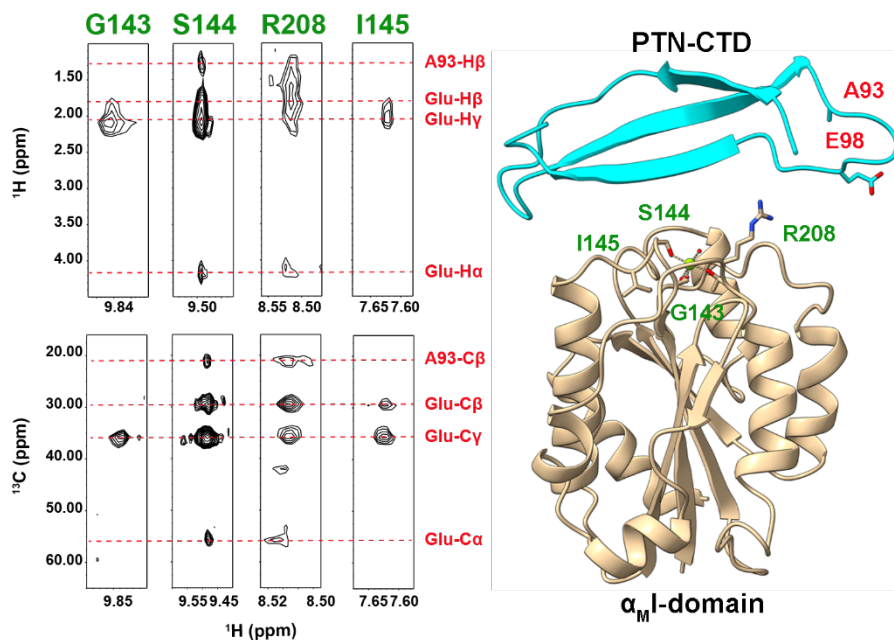
11

Figure 4. Contacts between backbone amide hydrogen of ^{2}H, ^{15}N-labeled active α_MI-domain and ^{13}C-labeled PTN-CTD seen in ^{1}H-^{1}H and ^{1}H-^{13}C projections of 4D ^{13}C-HSQC-NOESY-^{15}N-HMQC. The assignments of PTN-CTD atoms are labeled in red and the assignments of α_MI-domain atoms are labeled in green. Ribbon representations of active α_MI-domain and PTN-CTD with residues involved in the intermolecular contacts labeled are shown on the right. Due to degenerate chemical shifts, the glutamate cannot be assigned unambiguously.

To confirm that E98 is involved in metal chelation, we prepared several mutants of PTN-CTD. There are three acidic clusters in PTN-CTD, including E76/D78, E66/E98, and a string of four acidic amino acids in the unstructured C-terminal tail (E120/E127/E132/D136) (Figure 5B). We created PTN-CTD mutants missing one of the three clusters. We also mutated H95, which is in the 90s loop (residues R92 to K101 in PTN) and can potentially chelate metal ions. To monitor the binding, we titrated active α_MI-domain with different PTN-CTD mutants and estimated the K_d using signal intensity increases experienced by the ligand-bound species. The results show that the mutation of E98 reduced the affinity most significantly (Figure 5A and Table S2). In particular, the removal of E76/D78 and the C-terminal tail (PTN-CTD Δtail) had only a marginal effect on PTN-CTD affinity whereas the mutation of E98 alone led to more than 5 fold decrease in affinity. Although the H95S mutation did not change the affinity drastically, both H95S and E98Q mutations produced large changes in chemical shift perturbation patterns in active α_MI-domain when compared to wild-type PTN-CTD (Figure 5B and Table S3). This indicates that E98 and H95 are in the

binding interface. It is worth noting that the mutation of E98 alone was not sufficient to eliminate the binding. The mutation of other acidic clusters also produced small decreases in affinity, indicating that other acidic amino acids also act as the chelator.
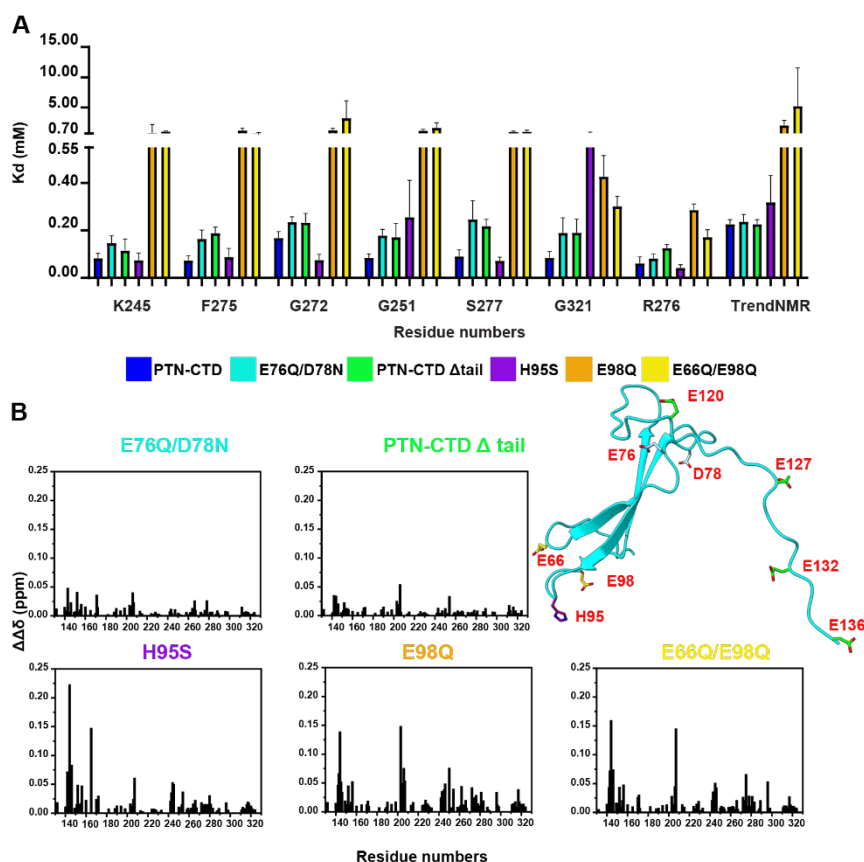

Figure 5. The effect of PTN mutations on its interactions with active α_MI-domain. (A) The K_d of the interaction between active α_MI-domain and PTN-CTD mutants. The K_ds were obtained by fitting the ligand induced intensity changes of either signals with high signal-to-noise ratio or by fitting the global spectral changes estimated using TRENDNMR. K_d for wild-type PTN-CTD is shown in blue, E76Q/D78N is shown in cyan, PTN-CTD Δtail is shown in lime, H95S is shown purple, E98Q is shown in orange, E66Q/E98Q is shown in yellow. Error bars reflect S. D. in data fitting. (B) Differences in active α_MI-domain backbone amide chemical shift changes induced by PTN-CTD mutants ($\Delta\Delta\delta$). The values were calculated by subtracting the chemical shift changes induced by the PTN-CTD mutant from the chemical shift changes induced by wild-type PTN-CTD. The ribbon representation of PTN-CTD with the mutated residues in the stick representation is shown on the right.

In addition to observing the effects of PTN-CTD mutations on the ^{15}N-edited HSQC spectrum of active α_MI-domain, we also examined the effect of H95 and E98 mutations on the PCS induced in PTN-CTD by Co^{2+}-bound active α_MI-domain. Figure 6A shows the impact of the mutations on the PCS signals of PTN-CTD residues with the strongest PCS peaks. The data revealed that the E98Q and H95S mutations

13

diminished the PCS signal intensities of these residues by more than 75 %. The effect of the mutation of another acidic cluster, E76Q/D78N, on the PCS was far smaller. In particular, the PCS signal of W52 side chain indole Nε-Hε was not changed at all by the E76Q/D78N mutations. These data imply that both E98 and H95 are important to maintaining stable interactions needed to produce PCS signals.
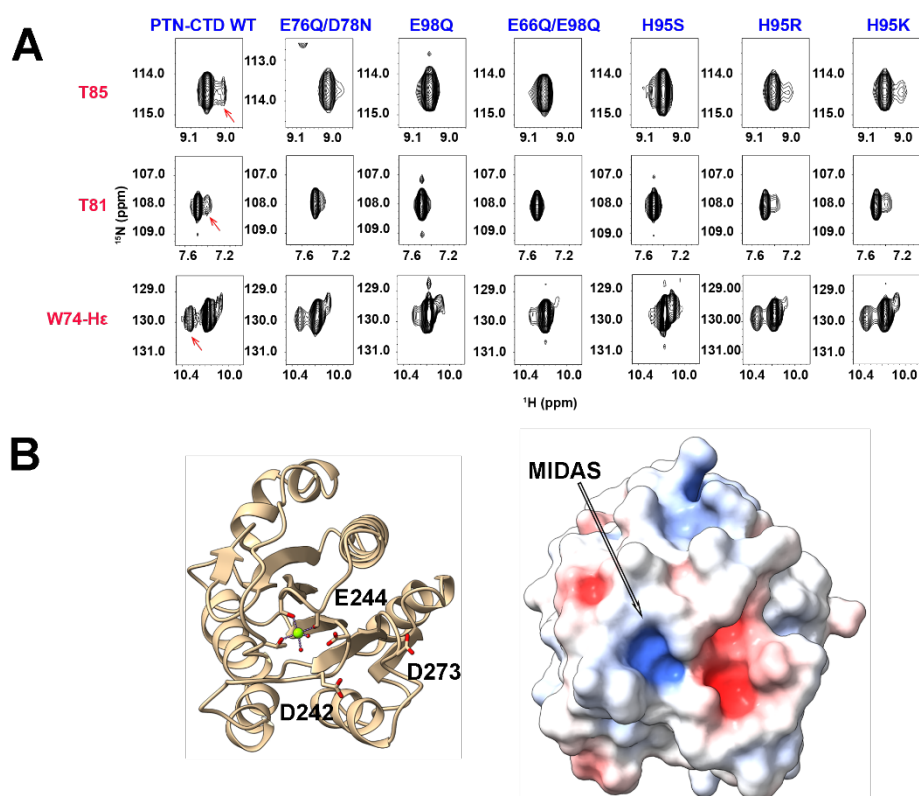

Figure 6. The role of H95 in binding active α_MI-domain. A) Effect of PTN-CTD mutations on PCS induced by Co^{2+}-bound active α_MI-domain. The mutation of E98Q, E66Q/E98Q and H95S drastically reduced the PCS of PTN-CTD residues. PCS signals of residues are indicated by red arrows. B) Ribbon (left) and surface (right) representations of active α_MI-domain. The Mg^{2+} ion in MIDAS is represented by the green sphere. Side chains of amino acids in the acidic patch are shown and labeled. Surface is colored based on the electrostatic surface potential range of -10 k_BT/e (red) to 10 k_BT/e (blue). Two representations are shown in the same orientation.

One question is how H95 interacts with MIDAS. We hypothesized that H95 in PTN-CTD interacts with the acidic pocket formed by α_MI-domain residues D242, E244, and D273 next to the MIDAS (Figure 6B), thereby stabilizing the interactions between E98 and active α_MI-domain. Similar stabilizing interactions between ligands and MIDAS of α I-domains were seen in the interactions of leukocidin GH and GP1bα with α_MI-domain as well as in the binding of ICAM-1 to α_LI-domain (Shimaoka et al., 2003;

14

Morgan et al., 2019; Trstenjak et al., 2020). To confirm this, we prepared H95K and H95R mutants of PTN-CTD. Replacing H95 with another basic amino acid would preserve the electrostatic interaction with the acidic pocket near MIDAS and the PCS resulting from this more stable interaction would be retained. Figure 6A shows the ^{15}N-HSQC spectra of H95K and H95R mutants of PTN-CTD in the presence of Co^{2+}-bound active α_MI-domain. The data demonstrate that, unlike the H95S mutation, substituting H95 with a basic amino acid preserves the PCS.

Modeling of the complexes formed by α_MI-domain and PTN domains. To model both Mg^{2+}-dependent and Mg^{2+}-independent interactions between PTN and α_MI-domain, we docked PTN domain structures onto the structure of either active or inactive α_MI-domain. We first confirmed that the structure of α_MI-domain was not changed significantly by PTN domains. To do this, we assessed the conformation of the PTN domain-bound α_MI-domain using the PCS induced in α_MI-domain by Co^{2+}. Our data show that the PCS of ligand-bound forms of both inactive and active α_MI-domain fit the crystal structures of free α_MI-domain well. In particular, the 81 PCS measured for the PTN-NTD bound inactive α_MI-domain fitted the crystal structure of inactive α_MI-domain (PDB ID 1JLM) with a Q factor of 0.055, and the ~ 30 PCS measured for the PTN-CTD bound active α_MI-domain fitted the crystal structure of active α_MI-domain (PDB ID 1IDO) with a Q factor of 0.071 (Figure S9). These data indicate that the crystal structures of both inactive and active α_MI-domain were a good starting point for modeling. For inactive α_MI-domain, we also obtained the Cα chemical shifts in the presence and absence of PTN-NTD. These chemical shifts are excellent predictors of secondary structures of the protein (Wishart et al., 1991, 1992; Wishart and Sykes, 1994). Analysis of the Cα chemical shifts showed the secondary structure of the protein has not changed (Figure S10). We also collected the backbone amide ^{1}H-^{15}N residual dipolar couplings (RDC) of α_MI-domain aligned in neutral polyacrylamide gel, both in the presence and absence of PTN-NTD. Although PTN-NTD appears to change the alignment of α_MI-domain, both sets of RDCs fit the crystal structure of inactive α_MI-domain (PDB code 1JLM) well (Conilescu Q factor of 0.25 and 0.28, respectively) (Figure S11). Because each PTN domain is small and

15

stabilized by multiple disulfide bonds, we do not expect interactions with α_MI-domain to change their structures.

To construct the model, we docked PTN-NTD onto inactive α_MI-domain using the program HADDOCK (Dominguez et al., 2003). The intermolecular NOEs were included as non-ambiguous distance constraints (Table S4). Loop residues identified as being in the interface (residues 260 to 266, 289 to 293 in α_MI-domain, and residues 25 to 27, 32 to 34, and 46 to 52 in PTN-NTD) were designated as flexible in the docking. The crystal structure of inactive α_MI-domain (PDB 1JLM) and the NMR structure of PTN-NTD (PDB 2N6F) were used as the starting structures. Clustering analysis of the 200 resulting models showed all models belonged to the same cluster. This indicates the NOE information is sufficient to determine the structure unambiguously. After superimposing the inactive α_MI-domain, the backbone RMSD of the structured region of PTN-NTD (residues 16 to 56) among the top 10 structures with the lowest overall HADDOCK scores was 1.9 Å. The docked structure shows the non-basic face of PTN-NTD and the loop formed by residues 26 to 34 contact the $\alpha5$-$\beta5$ and $\alpha6$-$\beta6$ loop in α_MI-domain (Figure 7). Besides hydrophobic contacts between L32 in PTN-NTD and I265 in α_MI-domain as well as between PTN's threonine methyls and P291 of α_MI-domain, there were also several polar and electrostatic interactions in the interface, including between R261 in α_MI-domain and D29 in PTN-NTD, R293 in α_MI-domain and E36 in PTN-NTD (Figure 7).

We also docked PTN-CTD onto active α_MI-domain using HADDOCK. A distance constraint between the MIDAS metal ion and the side chain of E98 was added based on crystal structures of active α_MI-domain with other ligands (Bajic et al., 2013; Jensen et al., 2016; Trstenjak et al., 2020). In addition, we also added distance constraints extracted from the NOESY data (Table S5). In particular, distance constraints between residues A93 in PTN-CTD and residues S144 and R208 in active α_MI-domain were used as well as constraints between E98 in PTN-CTD and residues G143, S144, I145, and R208 in active α_MI-domain. HADDOCK clustered the 200 resulting structures into three clusters. Approximately 150
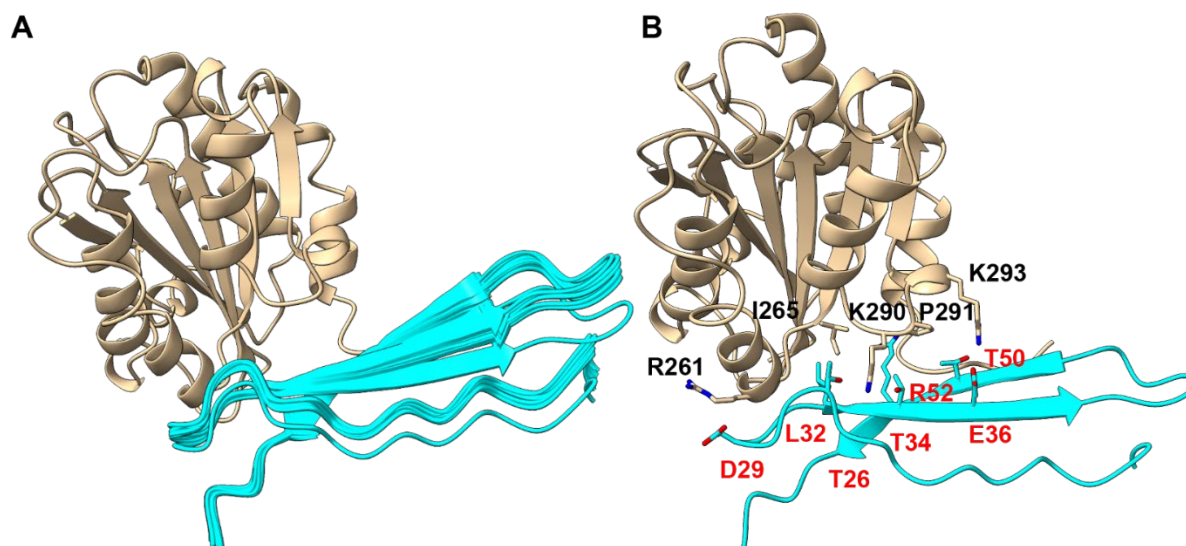
16

Figure 7. HADDOCK models of inactive α$_M$I-domain bound to PTN-NTD. (A) Top 10 models with lowest HADDOCK scores after superimposing α$_M$I-domain. The backbone RMSD of PTN-NTD is 1.9 Å. Only α$_M$I-domain from model 1 is shown. (B) One of the structures from the best 10 structures with the lowest HADDOCK score showing contacts in the binding interface between the proteins.

structures belonged to cluster 1. As expected, the main interaction is mediated by the 90s loop of PTN-CTD and MIDAS of α$_M$I-domain. However, significant heterogeneity exists in the orientation PTN-CTD adopts relative to α$_M$I-domain (Figure 8). As a result, the backbone RMSD for the structured portion of PTN-CTD (residues 66 to 109) after superimposing α$_M$I-domain is 3.9 Å. Even though no distance constraints were specified between H95 of PTN-CTD and any residue in active α$_M$I-domain, H95 was hydrogen bonded to the acidic amino acids in the acidic pocket formed by D242, E244, and D273 in active α$_M$I-domain in some of the structures.

To investigate the stability and validity of the models, we carried out a 500-ns MD simulation of the complexes in explicit solvents using the software AMBER (Case et al., 2005). Figure 9A shows the RMSF of PTN-NTD backbone relative to the starting structure after superimposing the inactive α$_M$I-domain backbone. Although a small shift in the position of the PTN-NTD at the beginning of the simulation was seen, PTN-NTD remained in stable contact with α$_M$I-domain during the simulation. The RMSF of the PTN-NTD backbone for the last 100 ns of the simulation was only ~ 2 Å (Figure 9A). In addition, the simulation revealed that the C-terminus of inactive α$_M$I-domain can have significant electrostatic interactions with

17

basic amino acids in PTN-NTD. In particular, residue E320 in inactive α_MI-domain had strong interactions with both K49 and R52 in PTN-NTD, D294 in inactive α_MI-domain hydrogen bonded to R52 in PTN-NTD, and the C-terminal carboxyl group of α_MI-domain has interactions with K54 in PTN-NTD (Figure 9D, frame 1). The residues in the C-terminus of α_MI-domain experienced significant PTN-induced chemical shift changes (Feng et al., 2021). However, NMR data showed no intermolecular NOEs between these residues and PTN-NTD. Results from the MD simulation indicate that the chemical shift perturbations may be due to dynamic electrostatic interactions between the C-terminus and the basic patch on PTN-NTD.
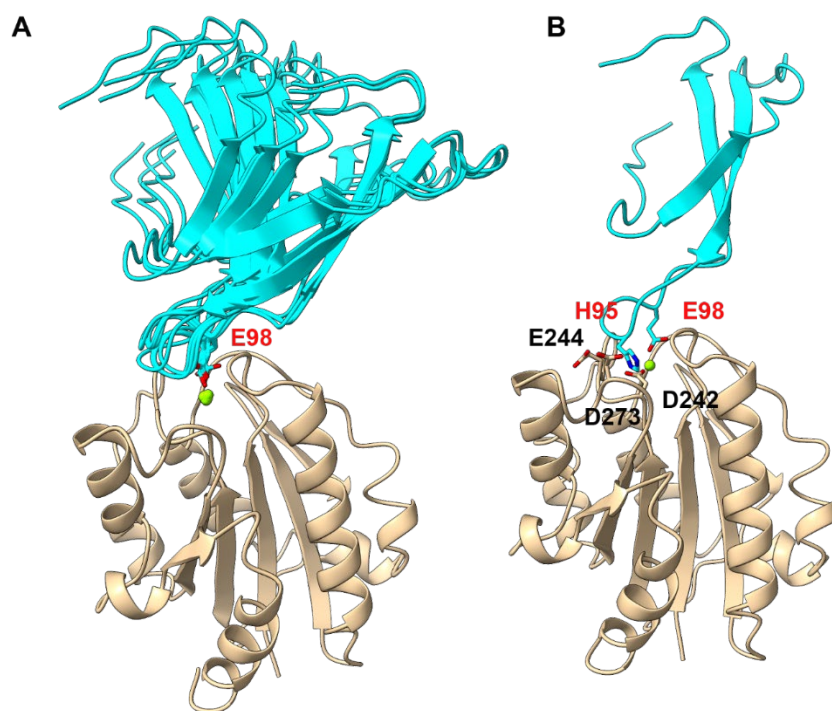

Figure 8. HADDOCK models of active α_MI-domain bound to PTN-CTD. (A) Top 10 models with the lowest HADDOCK scores in cluster 1. The α_MI-domain in the structures were superimposed. The backbone RMSD of PTN-CTD is 3.9 Å while the backbone RMSD of the binding loop (residues 92 to 101) is 2.5 Å. Only α_MI-domain from model 1 is shown. (B) One of the structures with H95 close to the acidic pocket formed by D273, D242 and E244.

Similar MD simulations of PTN-CTD-bound to active α_MI-domain were also carried out. We used a model with H95 in the acidic pocket as our starting structure. Similar to the HADDOCK results, PTN-CTD was considerably more dynamic than PTN-NTD in the simulation (Figure 9A). In particular, although the interaction of E98 with the MIDAS metal remained stable, the main body of PTN-CTD rotated by close to ~35 ° before gaining stability (Figure 9B), causing H95 to to loss contact with the acidic pocket on the

18

surface. However, the rotation allowed E66 of PTN-CTD to have electrostatic interactions with R208 in α_MI-domain, compensating for the loss of H95's interaction with α_MI-domain (Figure 9C & 9D).
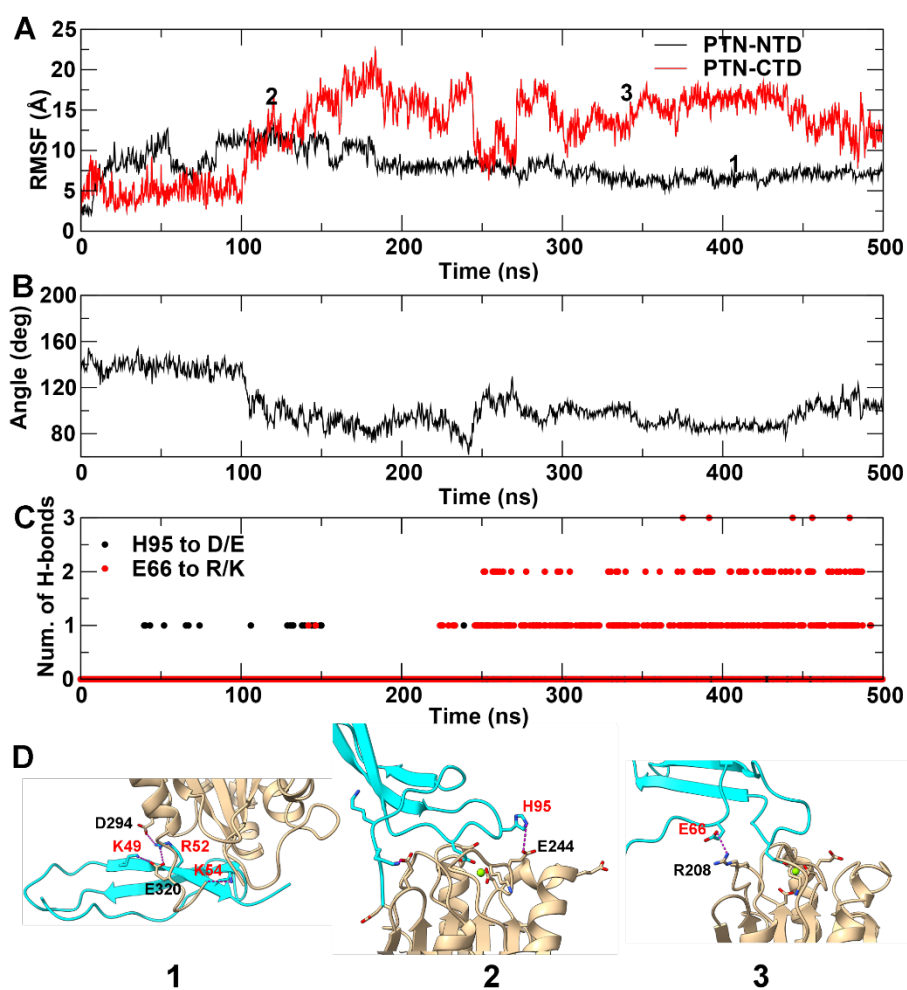

Figure 9. MD simulations of the models of PTN-NTD bound to inactive α_MI-domain and PTN-CTD bound to active α_MI-domain. A) RMSF of PTN-NTD and PTN-CTD structured regions relative to the starting structures after superimposing the α_MI-domain. B) Changes in the orientation of PTN-CTD relative to α_MI-domain during the simulation. The orientation is estimated by the angle between the vectors formed by the β1 strand in active α_MI-domain (residues 133 to 140) and the middle β strand in PTN-CTD (residues 84 to 91). C) Intermolecular hydrogen bonds between H95 in PTN-CTD and Asp/Glu in α_MI-domain (black), and E66 in PTN-CTD and Arg/Lys in α_MI-domain (red) during the simulation of active α_MI-domain bound to PTN-CTD. D) Frames from the simulations. 1. PTN-NTD's basic face interacting with the C-terminus α_MI-domain. 2. PTN-CTD's H95 interacting with acidic amino acids near MIDAS. 3. PTN-CTD's E66 interacting with R208 near the MIDAS. The positions of the frames in the simulations are marked with the frame numbers in panel A.

DISCUSSION

In this study, we investigated the interaction of α_MI-domain with PTN. Our data indicate that the α_MI-domain can have both metal-dependent and metal-independent interactions with PTN. The metal-independent interaction is dominated by the binding of PTN-NTD to the bottom of α_MI-domain and has fast time scale dynamics (Feng et al., 2021). This interaction also appears to be independent of the activation state of α_MI-domain. The metal-mediated binding is between PTN-CTD and active α_MI-domain. Its binding kinetics falls into the slow NMR time scale.

We previously reported that PTN-NTD is responsible for binding the inactive α_MI-domain in a metal-independent fashion (Feng et al., 2021). In this study, we determined the high-resolution structure of the complex. The data revealed that, besides the $\alpha5$-$\beta5$ loop, the $\alpha6$-$\beta6$ loop of inactive α_MI-domain also has extensive interactions with PTN-NTD. In particular, L32 of PTN-NTD contacts residues in the $\alpha5$-$\beta5$ loop of inactive α_MI-domain, with I265 being the most prominent residue in these interactions. Three threonines on one face of NTD also have extensive interactions with residues K290 and P291 in the $\alpha6$-$\beta6$ loop. Finally, the side chain of R52 in PTN-NTD also contacted I265 from inactive α_MI-domain. These contacts enabled us to model the structure of the complex using HADDOCK. Furthermore, MD simulations of the complex provided insight into why PTN perturbed the C-terminus of inactive α_MI-domain. In particular, the simulation showed that the basic face of PTN-NTD has extensive electrostatic interactions with the C-terminus of α_MI-domain. This explains the PTN-induced chemical shift perturbations previously observed in the C-terminus of inactive α_MI-domain (Feng et al., 2021).

Besides the metal-independent interaction between inactive α_MI-domain and PTN-NTD, our results indicate PTN-CTD can bind active α_MI-domain using the canonical metal-chelation mechanism. Although many PTN-CTD acidic amino acids can chelate the divalent cation in the MIDAS, the most stable metal chelator in PTN is residue E98. PTN's involvement in the metal-mediated binding mechanism is somewhat surprising because PTN's highly positive net charge makes it an ideal basic ligand, many of whom are known to bind using a metal-free mechanism (Yakubenko et al., 2001). However, the few acidic amino acids in basic ligands may be sufficient to chelate the metal. In addition, even though PTN is highly basic,

20

it does not have a significant amount of hydrophobic amino acids surrounding these basic amino acids, another feature required in the basic protein binding motif (Podolnikova et al., 2015b). Therefore, it may be unable to take advantage of α_MI-domain's binding site for basic/hydrophobic ligands.

One interesting finding of the study is that no single acidic amino acid in PTN is essential to binding. This implies that active α_MI-domain does not chelate just one acidic amino acid in PTN but can interact with multiple acidic amino acids. Signs of heterogeneous binding modes were also reported for the interaction of denatured fibrinogen with active α_MI-domain as well as α_XI-domain (Vorup-Jensen et al., 2005). LL-37's interaction with active α_MI-domain also appears to be heterogeneous in SPR analysis (Zhang et al., 2016). The heterogeneity explains why the PCS and non-PCS signals coexist and the intensities of PCS signals are only about 11 % of the normal peak. In particular, this may reflect that PCS signals can only be produced when E98 is the metal chelator and active α_MI-domain doesn't always bind E98. E98's ability to produce PCS is most likely the result of other interactions stabilizing PTN's interaction with α_MI-domain when E98 is in the MIDAS. One contact that may contribute to this is the interaction between PTN's H95 and the acidic pocket near MIDAS formed by D242, E244, and D273. The importance of H95 was demonstrated by the fact that its mutation to serine produced significant changes in PTN-CTD induced chemical shift perturbations observed in the ^{15}N-HSQC spectrum of α_MI-domain. Mutating H95 to anything other than another basic amino acid also resulted in the loss of all PCS. Chelation of the MIDAS metal by other PTN acidic amino acids besides E98 makes this interaction impossible and can result in dynamics that average the PCS to zero. However, the small magnitude of PCS observed in PTN indicates that even the interaction mediated by E98 chelation may be dynamic. This agrees with HADDOCK modeling and MD simulation, both of which showed dynamic movements in PTN-CTD's interaction with active α_MI-domain when E98 is the chelator. It is worth noting that conformational dynamics were also observed in the crystal structure of the drug simvastatin bound to active α_MI-domain (Jensen et al., 2016).

H95 and E98 can also be viewed as forming a zwitterionic ligand. In this regard, the interaction of active α_MI-domain with PTN is akin to integrins that bind the zwitterionic RGD motif across two different domains in the α and β subunits. However, in the case of α_MI-domain, the binding sites for the positive and

negative ions are found on the same domain. In addition, α_MI-domain is not the only α I-domain with a preference for zwitterionic ligands. A homologous acidic pocket in the human α_LI-domain was shown to be crucial to the binding of the zwitterionic motif [34]ETPLPK[39] in ICAM-1 (Shimaoka et al., 2003). The same phenomenon likely exists in ICAM-1 and α_MI-domain binding. In particular, it has been proposed that D229 in D3 of ICAM-1 is most likely the metal chelator (Diamond et al., 1991; Mao et al., 2011). Interestingly, R231 is situated nearby and the side chains of D229 and R231 point in the same direction, enabling R231 to bind the acidic pocket of D242, E244, and D273 on α_MI-domain. Such zwitterionic interaction was also observed in leukocidin GH's interaction with α_MI-domain. In particular, R294 and K319 in leukocidin H bind the acidic pocket while E323 of leukocidin H chelates the metal in α_MI-domain (Trstenjak et al., 2020). The same phenomenon was also proposed for GP1bα's interaction with α_MI-domain with H220 in GP1bα playing the role of the basic amino acid while E224 chelates the metal (Morgan et al., 2019). In addition, the removal of K39 in ICAM-1, K319 in leukocidin H, and H220 in GP1bα significantly reduced the binding of the respective ligand to α_MI-domain (Shimaoka et al., 2003; Morgan et al., 2019; Trstenjak et al., 2020). However, in the case of PTN, removing H95 only eliminated PCS experienced by PTN without changing the binding affinity. This suggests that H95's interaction with the acidic pocket may not be as strong as in other ligands. Factors such as the accessibility of E98, and the favorable interaction between residue E66 in PTN and residue R208 in α_MI-domain, may also contribute to α_MI-domain's preference for E98. It should be noted that other ligands also utilize residue R208 in their interaction with α_MI-domain. In particular, acidic amino acids in both C3d and leukocidin H have contacts with residue R208 in α_MI-domain. C3d also has electrostatic interactions with residues E178 and E179 located next to R208 (Bajic et al., 2013; Trstenjak et al., 2020). The emerging trend from these studies is that the charged residues around α_MI-domain's MIDAS play important roles in mediating interaction with ligands.

It should also be noted that the acidic pocket next to the MIDAS may serve as a ligand-binding site independent of the MIDAS. In particular, the acidic pocket can be an ideal binding site for basic proteins and peptides, which are known to have strong affinities for active α_MI-domain (Podolnikova et al., 2015b; Lishko et al., 2018). Although the binding site for most of the basic ligands has not been confirmed, a

previous study on the interaction between α_MI-domain and the archetypal basic α_MI-domain ligand, the peptide P2-C from fibrinogen, showed that mutations of residues around MIDAS significantly attenuated the binding of P2-C to α_MI-domain (Yakubenko et al., 2001). This strongly supports the proposal that basic ligands can bind to sites around MIDAS.

The finding that both PTN domains are involved in α_MI-domain binding suggests a mechanism by which PTN may cross-link cells to the extracellular matrix. In particular, because both domains of PTN can bind GAG as well as active α_MI-domain, it is plausible that one domain may bind GAG while the other binds α_MI-domain. It is also tempting to speculate whether NTD and CTD from the same molecule of PTN can simultaneously bind the MIDAS and N/C-termini sites. However, the short linker between NTD and CTD makes such a scenario sterically challenging. The finding that wild-type PTN's affinity for active α_MI-domain is no higher than that of PTN-CTD also supports the lack of simultaneous binding of α_MI-domain by both PTN domains from the same PTN molecule. In addition, PTN's binding site for active α_MI-domain does not overlap with PTN's GAG-binding site. This explains why a previous study has shown that PTN immobilized on proteoglycans can still support macrophage adhesion (Shen et al., 2017)

The electrostatic surface potentials of α_LI-domain and α_XI-domain are significantly different from that of α_MI-domain (Vorup-Jensen and Jensen, 2018). In particular, the α_LI-domain has a hydrophobic patch near its MIDAS in addition to the acidic pocket. This patch is absent in both α_MI-domain and α_XI-domain and may be the reason behind α_LI-domain's monospecificity. In particular, the hydrophobic patch helps to exclude solvent from the MIDAS of α_LI-domain, thereby strengthening the electrostatic interaction between the ligand and the divalent cation. This may be the reason behind α_LI-domain's high affinity for domain 1 of ICAM-1 (Shimaoka et al., 2003; San Sebastian et al., 2006). Similar hydrophobic interaction with other ligands may be a prerequisite for achieving strong affinity for α_LI-domain. The lack of this hydrophobic patch in α_MI-domain and α_XI-domain suggests that these domains may be less selective and would bind any charged ligands, albeit at lower affinity. This feature may partly explain ligand binding promiscuity exhibited by Mac-1. The ligand specificities of α_MI-domain and α_XI-domain are also not identical. The basis for this difference lie in the absence of the acidic pocket in α_XI-domain. The lack of an acidic pocket near

the MIDAS significantly enhances α_XI-domain's affinity for anionic polymers such as heparin and unfolded proteins compared to α_MI-domain or α_LI-domain (Vorup-Jensen et al., 2005). These differences may be the key to developing specific inhibitors for each α I-domain.

In summary, we have determined the interaction between PTN and α_MI-domain. We conclude that PTN can bind α_MI-domain using two different mechanisms depending on the activation state of α_MI-domain. When α_MI-domain is in the inactive state, PTN binds to the bottom side of α_MI-domain using PTN-NTD and a metal-independent mechanism. When α_MI-domain is in the active state, the interaction is dominated by the canonical metal-chelation mechanism in which PTN's residue E98 acts as the major chelator of the divalent cation in the MIDAS. In addition, the chelation of the metal by E98 is stabilized by favorable electrostatic interactions between PTN and active α_MI-domain residues near the MIDAS. We think these interactions are crucial to determining the ligand specificity of α_MI-domain.

KEY RESOURCES TABLE

REAGENT or RESOURCE	SOURCE	IDENTIFIER
Bacterial and virus strains		
Origami (DE3) competent *E. coli*	Novagen	70837
BL21 (DE3) competent *E. coli*	NEB	C2527H
Chemicals, peptides, and recombinant proteins		
Yeast Extract	Millipore Sigma	1138859010
Tryptone	VWR Life Science	97063-390
IPTG (Isopropyl ß-D-1-thiogalactopyranoside)	Fisher Science	BP1755-1
Ampicillin	Fisher Science	BP1760-5
Kanamycin	VWR Life Science	75856-684
Tetracyclin	Alfa Aesar	B21408.22
$^{15}NH_4Cl$	Cambridge Isotope Laboratories	NLM-467-PK
D_2O	Cambridge Isotope Laboratories	DLM-4-PK
^{13}C-labeled glucose	Cambridge Isotope Laboratories	CLM-1396-PK
Deuterated Celtone base powder	Cambridge Isotope Laboratories	CGM-1030P-C-0.5
Critical commercial assays		
Q5® Site-Directed Mutagenesis Kit	NEB	E0554
QIAGEN Plasmid Mini Kit	QIAGEN	12123
Deposited data		
Chemical shift assignments of Mg^{2+} species of the Q163C/Q309C α_MI-domain and unambiguous distance restraints used in HADDOCK docking of PTN-CTD.	BMRB	BMRB ID 31139
Chemical shift assignments of inactive α_MI-domain and unambiguous distance restraints used in HADDOCK docking of PTN-NTD.	BMRB	BMRB ID 31138
Coordinates of the top 10 HADDOCK models of the active α_MI-domain-PTN-CTD complex.	PDB	PDB ID 8VOI
Coordinates of the top 10 HADDOCK models of the inactive α_MI-domain-PTN-NTD complex.	PDB	PDB ID 8VOH
Oligonucleotides		
Primer		
PTN-CTD E66Q mutagenesis F: ATTTGGCGCGCAGTGCAAATACC R: TGCTTCTTCCAGTTGCAG	This manuscript	N/A
PTN-CTD E98Q mutagenesis F: GCACAATGCCCAGTGCCAGAAGAC R: AGGGCTCGCTTCAGAC	This manuscript	N/A
PTN-CTD E76Q/D78N mutagenesis F: GTAACCTGAACACAGCCCTGAAG R: ACTGTCCCCAGGCCTGGAAC	This manuscript	N/A
PTN-CTD H95S F: GCGAGCCCTGAGCAATGCCGAAT Q: TTCAGACTTCCAGTTCTGG	This manuscript	N/A

PTN-CTD H95K F: GCGAGCCCTGAAAAATGCCGAAT R: TTCAGACTTCCAGTTCTGGTC	This manuscript	N/A
PTN-CTD H95R F: GCGAGCCCTGCGCAATGCCGAAT R: TTCAGACTTCCAGTTCTGGTCTTCAGG	This manuscript	N/A
PTN-CTD clone into pHUE with *Sac*II/*Hind*III F:GGGCCGCGGTGGAAACTGGAAGAAGCAATTTG R: GGGAAGCTTCTAATCCAGCATCTTCTCCTGTT	This manuscript	N/A
Recombinant DNA		
pET-15b-PTN	Eathen Ryan et al (Ryan et al., 2016)	N/A
pHUE-PTN-NTD	Eathen Ryan et al (Ryan et al., 2016)	N/A
pHUE-PTN-CTD-Δtail	Eathen Ryan et al (Ryan et al., 2016)	N/A
pHUE CTD mutants (Δ tail, E76Q/D78N, H95S, E98Q, E66Q/E98Q, H95R, H95K)	This manuscript	N/A
pHUE-inactive α_MI-domain	Wei Feng et al. (Feng et al., 2021)	N/A
pHUE-active α_MI-domain Q163C/Q309C	Hoa Nguyen et al (Nguyen et al., 2023)	N/A
Software and algorithms		
nmrPipe	NIST IBBR	Website: https://www.ibbr.umd.edu/nmrpipe/
NMRViewJ	NMRFX	Website: https://nmrfx.org/nmrfx/nmrviewj
VMD	University of Illinois at Urbana-Chamipaign	Website: https://www.ks.uiuc.edu/Research/vmd/
ChimeraX	University of California San Francisco	Website: https://www.cgl.ucsf.edu/chimerax/
Paramagpy	Henry Orton, Australian National University.	https://henryorton.github.io/paramagpy/build/html/index.html
xcurvfit	Brian Sykes, University of Alberta	http://www.bionmr.ualberta.ca/bds/software/xcrvfit/latest/index.html

GraphPad Prism 9	Prism	https://www.graphpad.com/features
HADDOCK2.4	Utrecht University	https://wenmr.science.uu.nl/
AMBER22	UCSF	ambermd.org
Other		
HiTrap SP HP	Cytiva	17115401
HisTrap HP	Cytiva	17524802
HiLoad® 16/600 Superdex® 75 pg	Cytiva	GE28-9893-33
ÄKTA Pure system	Cytiva	29018224
Amicon® Ultra-15	Millipore Sigma	UFC901024
Amicon® Ultra-4	Millipore Sigma	UFC801024
AVANCE 600 MHz	Bruker	N/A
Avance II 850 MHz	Bruker	N/A
Inova 800 MHz	Agilent	N/A

METHOD DETAILS

Expression and Purification of α_MI-domains. The expression and purification of α_MI-domain were accomplished using the previously reported procedures (Feng et al., 2021; Nguyen et al., 2023). Briefly, the open reading frame (ORF) of the wild-type human α_MI-domain (E131-T324) was cloned into the pHUE vector (Catanzariti et al., 2004) using *Sac*II and *Hind*III as restriction sites. The activating Q163C/Q309C cysteine mutations were introduced into α_MI-domain using the Q5 Site-Directed Mutagenesis Kit (NEB). The plasmids were transformed into either BL21(DE3) (NEB) or OrigamiB(DE3) (Novagen) and the cells were grown in M9 media at 37 °C until the culture reached an OD_{600} of ~ 0.8-1. The protein expression was induced with 0.5 mM IPTG, and the cell pellet was harvested after overnight incubation at 22°C. The pellet was resuspended and incubated on ice in the lysis buffer (20 mM sodium phosphate, 0.5 M NaCl, 10 mM imidazole, 5% glycerol) containing 1 mg/ml lysozyme for 20 min on ice. After sonication and centrifugation, the supernatant was loaded onto a 5-mL HisTrap column (Cytiva), and the protein was eluted from the column by running a 0.01 to 0.5 M imidazole gradient. To separate His-ubiquitin from α_MI-domain, the protein was digested with enzyme USP2 (1:50 molar ratio) overnight at room temperature in 20 mM Tris, 0.1 M NaCl (Catanzariti et al., 2004). The digestion mixture was subjected to Ni^{2+} column purification again. α_MI-domain in the flow-through was further purified with a 120-mL Superdex 75 column using a

buffer containing 20 mM HEPES, 0.3 M NaCl, pH 7.0. Finally, the protein was exchanged into 20 mM HEPES, 0.1 M NaCl, pH 7.0 for NMR analyses. To prepare isotope labeled protein, ^{15}N, ^{13}C or ^{2}H labeling was accomplished by adding ^{15}NH$_4$Cl, ^{13}C glucose, D$_2$O, and deuterated Celtone base powder (Cambridge Isotope). The ^{2}H, ^{15}N-labeled α$_M$I-domain was prepared by seeding freshly transformed colony in 20 mL of LB until the OD$_{600}$ reached 1.0. Cells from 5 mL of the LB culture were gently pelleted, used to inoculate 50 mL of ^{2}H, ^{15}N minimal media, and grew overnight at 37 °C. The 50-mL culture was then used to seed 0.45 L of media the next day and grown as described before. The protein was expressed and harvested with the same procedure mentioned above.

Expression and Purification of PTN. PTN and its domains were produced following previously reported protocols (Feng et al., 2021). Briefly, the mature PTN open reading frame was cloned into a pET-15b vector using *Nco*I and *Xho*I restriction sites and transformed into OrigamiB(DE3) cells. The transformed cells were grown under conditions similar to the Q163C/Q309C mutant of the α$_M$I-domain. To extract the protein, cell pellets were resuspended in 20 mM Tris, 0.2 M NaCl, pH 8.0, 1 mg/mL of lysozyme and incubated for 20 minutes at room temperature. After sonication and centrifugation to remove insoluble material, the protein is extracted from the supernatant using a 5-mL HiTrap SP HP column (Cytiva) and eluted with a 0.1-1.5 M NaCl gradient. To produce PTN domains, a pHUE vector(Catanzariti et al., 2004) containing PTN ORF coding either residues G1 to C57 (PTN-NTD), residues N58 to K114 (PTN-CTD Δtail), or residues N58 to D136 (PTN-CTD) at the 3' end of the ubiquitin ORF was transformed into OrigamiB(DE3) cells. Cells were grown in M9 media at 37 °C to an OD$_{600}$ of 0.8. 0.25 mM IPTG was added to the culture and incubated overnight at 23°C. Purifications of PTN domains and various mutants were similar to that of α$_M$I-domain except no size exclusion chromatography was used.

NMR Data Acquisition. NMR data were collected on either Bruker AVANCE 600 MHz equipped with a Prodigy probe, a Bruker Avance II 850 MHz equipped with a cryoprobe, or an Agilent Inova 800 MHz equipped with a cold probe. All data were collected at 25 °C. Backbone assignments of PTN and Q163C/Q309C α$_M$I-domain were carried out previously (Ryan et al., 2016; Nguyen et al., 2023). For PTN

domain backbone and side chain assignment, CACBCONH, HNCACB, and HCCCONH were collected on ^{13}C, ^{15}N-labeled PTN-NTD and PTN-CTD. The parameter was set with 1024 complex points in ^{1}H dimension, 30 complex points in ^{15}N dimension, 50 complex points in ^{13}C dimension for 3D experiment. 2D ^{15}N-HSQC experiments were acquired with 1024 complex points in ^{1}H dimension and 50 complex points in the ^{15}N dimension with the spectrum widths are 15 ppm for ^{1}H dimension and 35 ppm for ^{15}N dimension with carrier at 4.7 and 119ppm, respectively.

Intermolecular NOEs between PTN-NTD and inactive α_MI-domain were obtained using F1-^{13}C-edited/F3-^{13}C,^{15}N-filtered HSQCNOESY experiments. The sample used to collect these data contained 0.2 mM ^{13}C-labeled inactive α_MI-domain and 1 mM unlabeled PTN-NTD. To confirm the assignments of PTN-NTD atoms at the interface, we acquired F1-^{13}C,^{15}N-filtered /F3-^{13}C-edited NOESYHSQC data on samples containing 0.2 mM unlabeled inactive α_MI-domain and 0.5 mM ^{13}C, ^{15}N-labeled PTN-NTD. To obtain intermolecular NOE between PTN-CTD and active α_MI-domain, we collected 2D projections of the ^{13}C HSQC - NOESY-^{15}N HMQC experiment on a sample containing 0.25 mM of ^{2}H,^{15}N-labeled Q163C/Q309C α_MI-domain and 1 mM ^{13}C PTN-CTD in 20 mM HEPES, 0.1 M NaCl, pH 7.0. The NOE mixing time is 0.2s.

Each titration of active α_MI-domain with PTN mutants was performed with a series of six samples. All samples in the series contained ~ 90 µM of ^{15}N-labeled active α_MI-domain. The PTN ligand concentrations in the samples are 0, 0.3 0.6, 0.9, 1.2 and 1.5 mM. ^{15}N-HSQC of each sample was acquired with the parameters described above.

To measure the α_MI-domain-induced chemical shift changes on PTN-NTD, ^{15}N HSQC spectra were acquired on a sample containing 0.1 mM of ^{15}N-labeled PTN-NTD and 0.8 mM of unlabeled inactive α_MI-domain or Q163C/Q309C α_MI-domain. The sample buffer is 20 mM HEPES, 0.1 M NaCl, pH 7.0. The chemical shift change of each signal was quantified using the equation $\delta=[\Delta\delta_H{}^2 + (0.17\,\Delta\delta_N)^2]^{1/2}$, where $\Delta\delta_H$ is the chemical shift change of amide hydrogen and $\Delta\delta_N$ is the chemical shift change of amide nitrogen.

To confirm that PTN does not induce significant changes in the structure of inactive α_MI-domain, an aligned sample of 0.1 mM ^{15}N α_MI-domain in a 6% neutral polyacrylamide gel (Cierpicki and Bushweller, 2004) was used to obtain HN residual dipolar coupling (RDC). The RDC of α_MI-domain were measured in the presence and absence of 0.8 mM unlabeled PTN-NTD.

To measure the pseudocontact shift (PCS) of α_MI-domain in the presence and absence of PTN-NTD and PTN-CTD, we collected ^{15}N-HSQC, HNCACB and CBCACONH spectra of Co^{2+}-saturated inactive α_MI-domain in the presence of unlabeled PTN-NTD and of Co^{2+}-saturated active α_MI-domain in the presence of unlabeled PTN-CTD. The NMR samples used to collect these data contained 0.2 mM ^{13}C, ^{15}N α_MI-domain, 1 mM unlabeled PTN-CTD or PTN-NTD, 2 mM of either $CoCl_2$ or $MgCl_2$, 20 mM HEPES, 0.1 M NaCl, pH 7.0. The amide hydrogen and nitrogen chemical shift assignments of α_MI-domain residues in the presence of Co^{2+} were obtained by comparing H, N, CA, CB chemical shifts of each spin system with the corresponding chemical shifts from residues in the Mg^{2+} sample. A match is made if the four chemical shifts from a spin system in the Co^{2+} data match the four chemical shifts from an assigned residue in the Mg^{2+} sample while taking into consideration the PCS on each atom as a result of the Co^{2+}. PCS tensors were calculated using the software Paramagpy (Orton et al., 2020) using only the PCS measured from amide hydrogens and PDB structures 1JLM (inactive α_MI-domain) or 1IDO (active α_MI-domain).

Modeling of PTN-α_MI-domain complexes. The model between α_MI-domain and PTN domains was generated using HADDOCK (Dominguez et al., 2003). Unambiguous contacts between α_MI-domain and PTN-NTD's residues obtained from F1-^{13}C-edited/F3-^{13}C,^{15}N-filtered HSQCNOESY spectra were used as constraints for the model (Table S4). For the complex between active α_MI-domain and PTN-CTD, contacts observed in the 4D ^{13}C-HSQC-NOESY-^{15}N-HMQC spectrum were used as constraints (Table S5). The crystal structure of inactive α_MI-domain (PDB accession number 1JLM) and the solution structure of PTN-NTD (PDB accession number 2N6F) were used as the starting structures to model the Mg^{2+}-independent interactions between α_MI-domain and PTN-NTD. The crystal structure of the active α_MI-domain (PDB accession number 1IDO) was used as the starting α_MI-domain structure to model the Mg^{2+}-dependent

interaction. During docking, we allowed the protein segments containing residues involved in binding to be fully flexible. For the modeling of Mg^{2+}-independent interaction, these residues include D260 to R266 and I287 to V296 from α_MI-domain, as well as P25 to S27, L32 to R34, and Q46 to R52 from PTN-NTD. For the modeling of Mg^{2+}-dependent interaction, flexible residues include G141 to I145 and L206 to R208 in α_MI-domain, and A93 to E98 in PTN-CTD. The docking followed the default protocol with an explicit solvent refinement for the last cycle. The best models were chosen based on HADDOCK energy scores and agreement with the constraints. Molecular dynamics (MD) simulations of the models were carried out using the top-scoring model from each docking study as the starting structure. For each simulation, the starting structure was first energy minimized. This was followed by a gradual heating to 300 K and then equilibration at 300 K with a 50 ps simulation. The production run was conducted with constant pressure and simulated with 1 fs step for 500 ns.

Resource Availability

Lead contact: Further information and requests for resources and reagents should be directed to and will be fulfilled by Xu Wang (xuwang@asu.edu).

Materials availability: All unique reagents generated in this study are available from the lead contact without restriction.

Data availability: HADDOCK models of the inactive α_MI-domain-PTN-NTD complex have been deposited as PDB entry 8VOH. HADDOCK models of the active α_MI-domain-PTN-CTD complex have been deposited as 8VOI. Restraints and chemical shifts used in the modeling have been deposited as BMRB entry 31138 for the inactive α_MI-domain-PTN-NTD complex and as BRMB entry 31139 for the active α_MI-domain-PTN-CTD complex.

ACKNOWLEDGEMENTS

Author Contribution

X.W. and T. U. conceived the project. X. W. and H. N. designed and conducted the experiments. X. W., H.N., N. P., and T. U. wrote the paper.

Declaration of interests

The authors have no competing interests.

REFERENCE

Altieri, D.C., Agbanyo, F.R., Plescia, J., Ginsberg, M.H., Edgington, T.S., and Plow, E.F. (1990). A unique recognition site mediates the interaction of fibrinogen with the leukocyte integrin Mac-1 (CD11b/CD18). The Journal of biological chemistry *265*, 12119-12122.

Bajic, G., Yatime, L., Sim, R.B., Vorup-Jensen, T., and Andersen, G.R. (2013). Structural insight on the recognition of surface-bound opsonins by the integrin I domain of complement receptor 3. Proceedings of the National Academy of Sciences of the United States of America *110*, 16426-16431.

Cai, T.Q., and Wright, S.D. (1996). Human leukocyte elastase is an endogenous ligand for the integrin CRR3 (CD11b/CD18, Mac-1, αMβ2) and modulates polymorphonuclear leukocyte adhesion. Journal of Experimental Medicine *184*, 1213-1223.

Case, D.A., Cheatham, T.E., 3rd, Darden, T., Gohlke, H., Luo, R., Merz, K.M., Jr., Onufriev, A., Simmerling, C., Wang, B., and Woods, R.J. (2005). The Amber biomolecular simulation programs. Journal of computational chemistry *26*, 1668-1688.

Catanzariti, A.M., Soboleva, T.A., Jans, D.A., Board, P.G., and Baker, R.T. (2004). An efficient system for high-level expression and easy purification of authentic recombinant proteins. Protein Science *13*, 1331-1339.

Cierpicki, T., and Bushweller, J.H. (2004). Charged gels as orienting media for measurement of residual dipolar couplings in soluble and integral membrane proteins. Journal of the American Chemical Society *126*, 16259-16266.

Coxon, A., Rieu, P., Barkalow, F.J., Askari, S., Sharpe, A.H., Von Andrian, U.H., Arnaout, M.A., and Mayadas, T.N. (1996). A novel role for the beta 2 integrin CD11b/CD18 in neutrophil apoptosis: a homeostatic mechanism in inflammation. Immunity *5*, 653-666.

Davis, G.E. (1992). The Mac-1 and p150,95 beta 2 integrins bind denatured proteins to mediate leukocyte cell-substrate adhesion. Experimental Cell Research *200*, 242-252.

Diamond, M.S., Staunton, D.E., de Fougerolles, A.R., Stacker, S.A., Garcia-Aguilar, J., Hibbs, M.L., and Springer, T.A. (1990). ICAM-1 (CD54)-a counter-receptor for MAC-1 (CD11b/CD18). Journal of Cell Biology *111*, 3129-3139.

Diamond, M.S., Staunton, D.E., Marlin, S.D., and Springer, T.A. (1991). Binding of the integrin Mac-1 (CD11b/CD18) to the third immunoglobulin-like domain of ICAM-1 (CD54) and its regulation by glycosylation. Cell *65*, 961-971.

Ding, Z.M., Babensee, J.E., Simon, S.I., Lu, H.F., Perrard, J.L., Bullard, D.C., Dai, X.Y., Bromley, S.K., Dustin, M.L., Entman, M.L*., et al.* (1999). Relative contribution of LFA-1 and Mac-1 to neutrophil adhesion and migration. Journal of Immunology *163*, 5029-5038.

Dominguez, C., Boelens, R., and Bonvin, A.M. (2003). HADDOCK: a protein-protein docking approach based on biochemical or biophysical information. Journal of the American Chemical Society *125*, 1731-1737.

Feng, W., Nguyen, H., Shen, D., Deng, H., Jiang, Z., Podolnikova, N., Ugarova, T., and Wang, X. (2021). Structural Characterization of the Interaction between the alphaMI-Domain of the Integrin Mac-1 (alphaMbeta2) and the Cytokine Pleiotrophin. Biochemistry *60*, 182-193.

Fernandez-Calle, R., Vicente-Rodriguez, M., Gramage, E., Pita, J., Perez-Garcia, C., Ferrer-Alcon, M., Uribarri, M., Ramos, M.P., and Herradon, G. (2017). Pleiotrophin regulates microglia-mediated neuroinflammation. Journal of neuroinflammation *14*, 46.

Fernandez, F.J., Santos-Lopez, J., Martinez-Barricarte, R., Querol-Garcia, J., Martin-Merinero, H., Navas-Yuste, S., Savko, M., Shepard, W.E., Rodriguez de Cordoba, S., and Vega, M.C. (2022). The crystal structure of iC3b-CR3 alphaI reveals a modular recognition of the main opsonin iC3b by the CR3 integrin receptor. Nature communications *13*, 1955.

Goldsmith, J.A., DiVenere, A.M., Maynard, J.A., and McLellan, J.S. (2022). Structural basis for non-canonical integrin engagement by Bordetella adenylate cyclase toxin. Cell reports *40*, 111196.

Jensen, M.R., Bajic, G., Zhang, X., Laustsen, A.K., Koldsø, H., Skeby, K.K., Schiøtt, B., Andersen, G.R., and Vorup-Jensen, T. (2016). Structural Basis for Simvastatin Competitive Antagonism of Complement Receptor 3*. Journal of Biological Chemistry *291*, 16963-16976.

Johansson, M.W., Patarroyo, M., Oberg, F., Siegbahn, a., and Nilsson, K. (1997). Myeloperoxidase mediates cell adhesion via the αMβ2 integrin (Mac-1, CD11b/CD18). Journal of Cell Science *110*, 1133-1139.

Lamers, C., Pluss, C.J., and Ricklin, D. (2021). The Promiscuous Profile of Complement Receptor 3 in Ligand Binding, Immune Modulation, and Pathophysiology. Frontiers in immunology *12*, 662164.

Lee, J.O., Bankston, L.A., Arnaout, M.A., and Liddington, R.C. (1995). Two conformations of the integrin A-domain (I-domain): a pathway for activation? Structure *3*, 1333-1340.

Linnerbauer, M., Losslein, L., Farrenkopf, D., Vandrey, O., Tsaktanis, T., Naumann, U., and Rothhammer, V. (2021). Astrocyte-Derived Pleiotrophin Mitigates Late-Stage Autoimmune CNS Inflammation. Frontiers in immunology *12*, 800128.

Lishko, V.K., Moreno, B., Podolnikova, N.P., and Ugarova, T.P. (2016). Identification of Human Cathelicidin Peptide LL-37 as a Ligand for Macrophage Integrin alphaMbeta2 (Mac-1, CD11b/CD18) that Promotes Phagocytosis by Opsonizing Bacteria. The Journal of biological chemistry *2016*, 39-55.

Lishko, V.K., Novokhatny, V., Yakubenko, V.P., Skomorovska-Prokvolit, H., and Ugarova, T.P. (2004). Characterization of plasminogen as an adhesive ligand for integrins αMβ2 (Mac-1) and α5β1 (VLA-5). Blood *104*, 719-726.

Lishko, V.K., Yakubenko, V.P., Ugarova, T.P., and Podolnikova, N.P. (2018). Leukocyte integrin Mac-1 (CD11b/CD18, alphaMbeta2, CR3) acts as a functional receptor for platelet factor 4. The Journal of biological chemistry *293*, 6869-6882.

Lu, C.F., and Springer, T.A. (1997). The α subunit cytoplasmic domain regulates the assembly and adhesiveness of integrin lymphocyte function-associated antigen-1. Journal of Immunology *159*, 268-278.

Mao, D., Lu, S., Li, N., Zhang, Y., and Long, M. (2011). Conformational stability analyses of alpha subunit I domain of LFA-1 and Mac-1. PloS one *6*, e24188.

Miao, J., Wang, F., Wang, R., Zeng, J., Zheng, C., and Zhuang, G. (2019). Pleiotrophin regulates functional heterogeneity of microglia cells in EAE animal models of multiple sclerosis by activating CCr-7/CD206 molecules and functional cytokines. American journal of translational research *11*, 2013-2027.

Michishita, M., Videm, V., and Arnaout, M.A. (1993). A novel divalent cation-binding site in the A domain of the beta 2 integrin CR3 (CD11b/CD18) is essential for ligand binding. Cell *72*, 857-867.

Morgan, J., Saleem, M., Ng, R., Armstrong, C., Wong, S.S., Caulton, S.G., Fickling, A., Williams, H.E.L., Munday, A.D., López, J.A*., et al.* (2019). Structural basis of the leukocyte integrin Mac-1 I-domain interactions with the platelet glycoprotein Ib. Blood advances *3*, 1450-1459.

Nguyen, H., Jing, T., and Wang, X. (2023). The Q163C/Q309C mutant of alphaMI-domain is an active variant suitable for NMR characterization. PloS one *18*, e0280778.

Nitsche, C., and Otting, G. (2017). Pseudocontact shifts in biomolecular NMR using paramagnetic metal tags. Prog Nucl Magn Reson Spectrosc *98-99*, 20-49.

Orton, H.W., Huber, T., and Otting, G. (2020). Paramagpy: software for fitting magnetic susceptibility tensors using paramagnetic effects measured in NMR spectra. Magn. Reson. *1*, 1-12.

Podolnikova, N.P., Brothwell, J.A., and Ugarova, T.P. (2015a). The opioid peptide dynorphin A induces leukocyte responses via integrin Mac-1 (alphaMbeta2, CD11b/CD18). Molecular pain *11*, 33.

Podolnikova, N.P., Hlavackova, M., Wu, Y., Yakubenko, V.P., Faust, J., Balabiyev, A., Wang, X., and Ugarova, T.P. (2019). Interaction between the integrin Mac-1 and signal regulatory protein alpha (SIRPalpha) mediates fusion in heterologous cells. The Journal of biological chemistry *294*, 7833-7849.

Podolnikova, N.P., Podolnikov, A.V., Haas, T.A., Lishko, V.K., and Ugarova, T.P. (2015b). Ligand recognition specificity of leukocyte integrin alphaMbeta2 (Mac-1, CD11b/CD18) and its functional consequences. Biochemistry *54*, 1408-1420.

Prince, J.E., Brayton, C.F., Fosset, M.C., Durand, J.A., Kaplan, S.L., Smith, C.W., and Ballantyne, C.M. (2001). The differential roles of LFA-1 and Mac-1 in host defense against systemic infection with Streptococcus pneumoniae. Journal of Immunology *166*, 7362-7369.

Rosetti, F., and Mayadas, T.N. (2016). The many faces of Mac-1 in autoimmune disease. Immunological reviews *269*, 175-193.

Ryan, E., Shen, D., and Wang, X. (2016). Structural studies reveal an important role for the pleiotrophin C-terminus in mediating interactions with chondroitin sulfate. The FEBS journal *283*, 1488-1503.

San Sebastian, E., Mercero, J.M., Stote, R.H., Dejaegere, A., Cossio, F.P., and Lopez, X. (2006). On the affinity regulation of the metal-ion-dependent adhesion sites in integrins. Journal of the American Chemical Society *128*, 3554-3563.

Santoso, S., Sachs, U.J., Kroll, H., Linder, M., Ruf, A., Preissner, K.T., and Chavakis, T. (2002). The junctional adhesion molecule 3 (JAM-3) on human platelets is a counterreceptor for the leukocyte integrin Mac-1. J.Exp.Med *196*, 679-691.

Schober, J.M., Lau, L.F., Ugarova, T.P., and Lam, S.C. (2003). Identification of a Novel Integrin αMβ2 Binding Site in CCN1 (CYR61), a Matricellular Protein Expressed in Healing Wounds and Atherosclerotic Lesions. Journal of Biological Chemistry *278*, 25808-25815.

Shappell, S.B., Toman, C., Anderson, D.C., Taylor, A.A., Entman, M.L., and Smith, C.W. (1990). Mac-1 (CD11b/CD18) mediates adherence-dependent hydrogen peroxide production by human and canine neutrophils. Journal of Immunology *144*, 2702-2711.

Shen, D., Podolnikova, N.P., Yakubenko, V.P., Ardell, C.L., Balabiyev, A., Ugarova, T.P., and Wang, X. (2017). Pleiotrophin, a multifunctional cytokine and growth factor, induces leukocyte responses through the integrin Mac-1. The Journal of biological chemistry *292*, 18848-18861.

Shimaoka, M., Lu, C., Salas, A., Xiao, T., Takagi, J., and Springer, T.A. (2002). Stabilizing the integrin αM inserted domain in alternative conformations with a range of engineered disulfide bonds. Proceedings of the National Academy of Sciences *99*, 16737-16741.

Shimaoka, M., Xiao, T., Liu, J.H., Yang, Y., Dong, Y., Jun, C.D., McCormack, A., Zhang, R., Joachimiak, A., Takagi, J.*, et al.* (2003). Structures of the alpha L I domain and its complex with ICAM-1 reveal a shape-shifting pathway for integrin regulation. Cell *112*, 99-111.

Simon, D.I., Chen, Z.P., Xu, H., Li, C.Q., Dong, J.F., McIntire, L.V., Ballantyne, C.M., Zhang, L., Furman, M.I., Berndt, M.C.*, et al.* (2000). Platelet glycoprotein Ibα is a counterreceptor for the leukocyte integrin Mac-1 (CD11b/CD18). Journal of Experimental Medicine *192*, 193-204.

Smith, C.W., Marlin, S.D., Rothlein, R., Toman, C., and Anderson, D.C. (1989). Cooperative interactions of LFA-1 and Mac-1 with intercellular adhesion molecule-1 in facilitating adherence and transendothelial migration of human neutrophils in vitro. The Journal of clinical investigation *83*, 2008-2017.

Trstenjak, N., Milic, D., Graewert, M.A., Rouha, H., Svergun, D., Djinovic-Carugo, K., Nagy, E., and Badarau, A. (2020). Molecular mechanism of leukocidin GH-integrin CD11b/CD18 recognition and species specificity. Proceedings of the National Academy of Sciences of the United States of America *117*, 317-327.

Ugarova, T.P., Solovjov, D.A., Zhang, L., Loukinov, D.I., Yee, V.C., Medved, L.V., and Plow, E.F. (1998). Identification of a novel recognition sequence for integrin α M β 2 within the gamma-chain of fibrinogen. Journal of Biological Chemistry *273*, 22519-22527.

Vorup-Jensen, T., Carman, C.V., Shimaoka, M., Schuck, P., Svitel, J., and Springer, T.A. (2005). Exposure of acidic residues as a danger signal for recognition of fibrinogen and other macromolecules by integrin alphaXbeta2. Proceedings of the National Academy of Sciences of the United States of America *102*, 1614-1619.

Vorup-Jensen, T., and Jensen, R.K. (2018). Structural Immunology of Complement Receptors 3 and 4. Frontiers in immunology *9*, 2716.

Wang, X. (2020). Pleiotrophin: Activity and mechanism. Advances in clinical chemistry *98*, 51-89.

Wishart, D.S., and Sykes, B.D. (1994). The 13C chemical-shift index: a simple method for the identification of protein secondary structure using 13C chemical-shift data. Journal of biomolecular NMR *4*, 171-180.

Wishart, D.S., Sykes, B.D., and Richards, F.M. (1991). Relationship between nuclear magnetic resonance chemical shift and protein secondary structure. Journal of molecular biology *222*, 311-333.

Wishart, D.S., Sykes, B.D., and Richards, F.M. (1992). The chemical shift index: a fast and simple method for the assignment of protein secondary structure through NMR spectroscopy. Biochemistry *31*, 1647-1651.

Wolf, D., Hohmann, J.D., Wiedemann, A., Bledzka, K., Blankenbach, H., Marchini, T., Gutte, K., Zeschky, K., Bassler, N., Hoppe, N.*, et al.* (2011). Binding of CD40L to Mac-1's I-domain involves the EQLKKSKTL motif and mediates leukocyte recruitment and atherosclerosis--but does not affect immunity and thrombosis in mice. Circulation research *109*, 1269-1279.

Xiong, J.P., Li, R., Essafi, M., Stehle, T., and Arnaout, M.A. (2000). An isoleucine-based allosteric switch controls affinity and shape shifting in integrin CD11b A-domain. The Journal of biological chemistry *275*, 38762-38767.

Xu, J., and Van Doren, S.R. (2016). Binding Isotherms and Time Courses Readily from Magnetic Resonance. Analytical chemistry *88*, 8172-8178.

Yakubenko, V.P., Solovjov, D.A., Zhang, L., Yee, V.C., Plow, E.F., and Ugarova, T.P. (2001). Identification of the binding site for fibrinogen recognition peptide g 383-395 within the αM I-domain of integrin αMβ2 Journal of Biological Chemistry *275*, 13995-14003.

Zhang, L., and Plow, E.F. (1996). Overlapping, but not identical, sites are involved in the recognition of C3bi, neutrophil inhibitory factor, and adhesive ligands by the alphaMbeta2 integrin. The Journal of biological chemistry *271*, 18211-18216.

Zhang, X., Bajic, G., Andersen, G.R., Christiansen, S.H., and Vorup-Jensen, T. (2016). The cationic peptide LL-37 binds Mac-1 (CD11b/CD18) with a low dissociation rate and promotes phagocytosis. Biochimica et Biophysica Acta (BBA) - Proteins and Proteomics *1864*, 471-478.